

# Photoelectric Detection of Nitrogen-Vacancy Centers Magnetic Resonances in Diamond: Role of Charge Exchanges with Other Optoelectrically Active Defects

Emilie Bourgeois,\* Josef Soucek,\* Jaroslav Hruby,\* Michal Gulka,\* and Milos Nesladek\*

The photoelectric detection of nitrogen-vacancy (NV) magnetic resonance (PDMR) in diamond, used for spin state detection and based on reading the photocurrent resulting from NV ionization, offers physical and technical advantages for the development of miniaturized and scalable quantum sensors, as well as solid-state quantum information devices integrated with electronics. Charge exchanges between NV centers and other optoelectrically active defects in diamond are an essential part of the PDMR scheme, impacting the spin-state control and the performances of the photoelectric readout. Through experimental characterization and modeling, processes governing the spin-state contrast, in particular the hole carrier contribution to the photocurrent and the role of acceptor-type defects are discussed. Such acceptor defects can act as traps for free electrons resulting from NV photoionization. Consequently, the hole current can increase at resonance, ultimately leading to an inversion of the sign of PDMR resonances, i.e. to a positive spin contrast. Based on these findings, a method to improve PDMR performances in terms of spin contrast and photoelectric detection rate by selectively ionizing low-energy acceptor defects using a bias red illumination is proposed. This method is shown to lead to a significant improvement of the photoelectric spin detection sensitivity, important for future practical devices.

## 1. Introduction

Thanks to its long spin coherence time and outstanding optical and magnetic properties, the negatively charged nitrogen-vacancy (NV<sup>-</sup>) center in diamond is considered as one of the most promising solid-state room temperature qubit platforms. Its applications range from quantum computing and communication to quantum sensing— including magnetometry,<sup>[1,2]</sup> electric field sensing,<sup>[3,4]</sup> thermometry<sup>[5,6]</sup> and detection of external electron<sup>[7,8]</sup> or nuclear spins.<sup>[9]</sup> Ultra-sensitive magnetic field sensing was in particular demonstrated using large NV ensembles.<sup>[10]</sup>


All applications of NV centers in the field of quantum technologies rely on the readout of NV<sup>-</sup> electron spin. The photoelectric detection of NV<sup>-</sup> magnetic resonances (PDMR) has been developed as an alternative to the optical readout of NV spin (Figure 1a),<sup>[11–16]</sup> making possible to determine NV electron spin state through detection of the photocurrent resulting from NV centers

two-photon ionization (Figure 1b). The PDMR technique, recently downscaled to the readout of a single coherently manipulated electronic<sup>[17]</sup> or nuclear<sup>[18]</sup> spin, presents potential advantages in terms of spatial resolution, detection rates, compactness, and integration with electronics<sup>[11–14]</sup> compared to the optical detection of magnetic resonances (ODMR).

The shot-noise limited sensitivity of NV-based quantum sensors to external fields is inversely proportional to the product between the root mean square of the detection rate and the electron spin contrast.<sup>[1,19]</sup> Optimizing PDMR performances in terms of the magnetic resonance contrast and photoelectric detection rate requires a deep understanding of the influence of defects other than NV centers on the PDMR process, especially in the case of dense NV ensembles used for the development of highly sensitive diamond sensors. Indeed, diamonds containing NV centers, in particular when they are prepared by high-energy irradiation and annealing of nitrogen-doped crystals, contain many other optoelectrically active defects, such as the substitutional nitrogen N<sub>S</sub>, the single vacancy V, the di-vacancy V<sub>2</sub>, interstitial atoms, and various complexes combining vacancies and nitrogen or hydrogen atoms (e.g., NVH or NVN). All these crystal defects can be photoionized and act as electron donors or acceptors,

E. Bourgeois, J. Soucek, J. Hruby, M. Gulka, M. Nesladek  
Hasselt University  
Martelarenlaan 42, Hasselt B-3500, Belgium  
E-mail: emilie.bourgeois@uhasselt.be; josef.soucek@uhasselt.be;  
jaroslav.hruby@uhasselt.be; gulka.michal@gmail.com;  
milos.nesladek@uhasselt.be

E. Bourgeois, J. Soucek, J. Hruby, M. Gulka, M. Nesladek  
IMEC Division  
IMEC  
Kapeldreef 75, Leuven B-3001, Belgium  
J. Soucek, M. Gulka, M. Nesladek  
Faculty of Biomedical Engineering  
Czech Technical University in Prague  
Sitna sq. 3105, Kladno 27201, Czech Republic

 The ORCID identification number(s) for the author(s) of this article can be found under <https://doi.org/10.1002/qute.202100153>

© 2022 The Authors. Advanced Quantum Technologies published by Wiley-VCH GmbH. This is an open access article under the terms of the Creative Commons Attribution-NonCommercial-NoDerivs License, which permits use and distribution in any medium, provided the original work is properly cited, the use is non-commercial and no modifications or adaptations are made.

DOI: 10.1002/qute.202100153

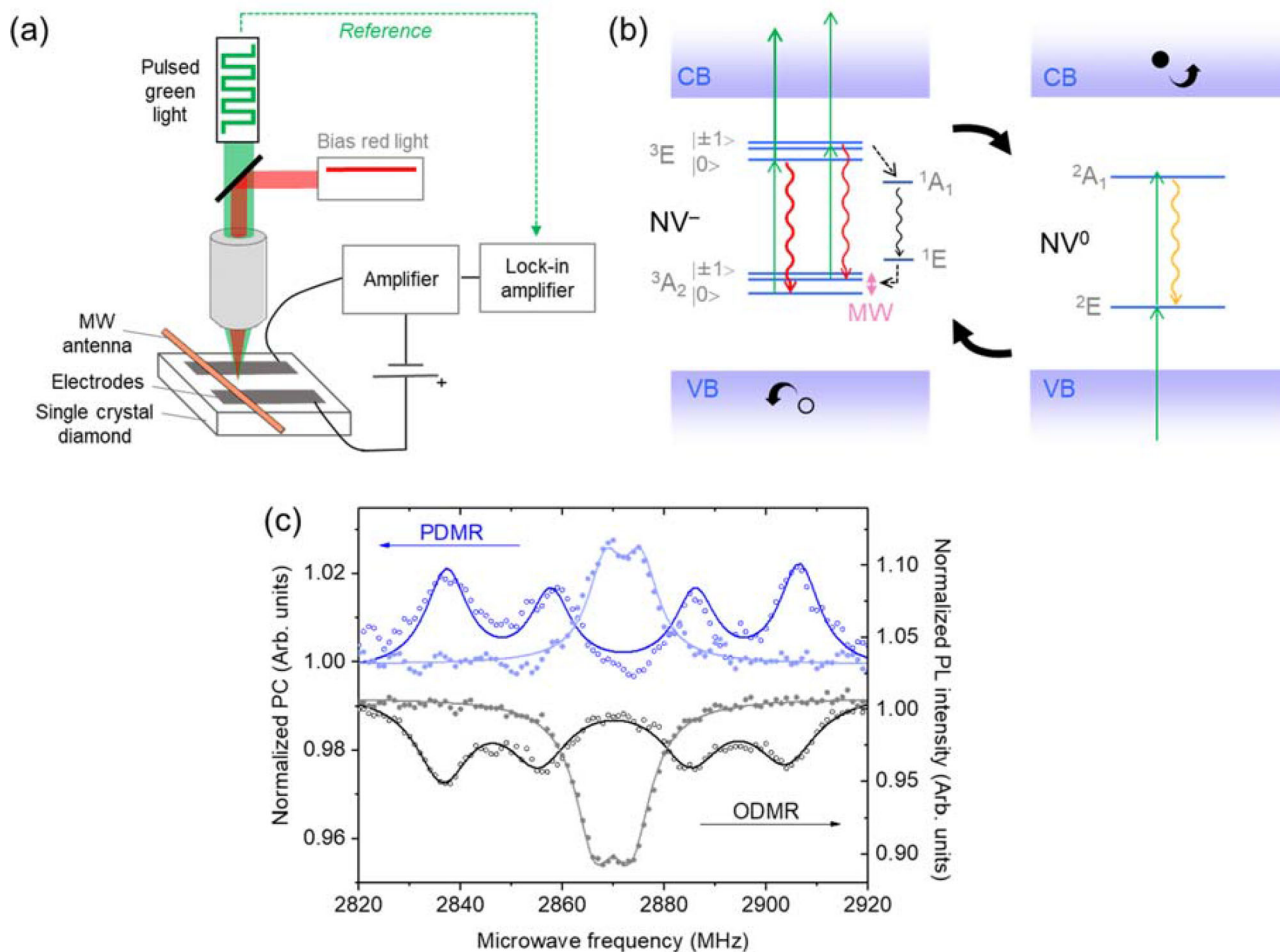


**Figure 1.** a) Schematic representation of the photoelectric detection of nitrogen-vacancy (NV) magnetic resonance (PDMR) setup. Green laser light (532 nm) pulsed at a low frequency is used to induce the two-photon ionization of NV<sup>-</sup> and the back-conversion from NV<sup>0</sup> to NV<sup>-</sup>. After amplification by a low-noise current-to-voltage amplifier, the photocurrent induced by NV ionization is detected by lock-in amplification, referenced to the green light pulsing frequency. Addition of a red bias light (660 nm) can be used to improve the PDMR contrast and photocurrent signal, as detailed in Section 4. b) NV<sup>-</sup> and NV<sup>0</sup> electronic structure in terms of multielectron levels, and principle of PDMR under green illumination. NV<sup>-</sup> two-photon ionization (straight green arrows), leads to the formation of free electrons in the conduction band (CB). The spin-dependent dynamics of this ionization process, due to spin-selective intersystem crossing (ISC) from the triplet excited state <sup>3</sup>E to the singlet state <sup>1</sup>A<sub>1</sub> (dashed black arrows), leads to the PDMR contrast. Photoluminescent transitions (red wavy arrows) from the <sup>3</sup>E state to <sup>3</sup>A<sub>2</sub> are detected in optical detection of magnetic resonance (ODMR). The two-photon back-conversion from NV<sup>0</sup> to NV<sup>-</sup> leads to the formation of holes in the valence band (VB). c) PDMR and ODMR spectra simultaneously measured on sample 6, in conditions leading to positive PDMR resonances (green laser power: 8 mW, focusing depth: 13.5 μm). Measurement performed without external magnetic field (full symbols) and in the presence of an external magnetic field aligned along the 111 axis of the crystal (empty symbols). Scattered points: experimental data. Full lines: Fit to the sum of two or four Lorentzian functions.

depending on their charge state. The presence of defects acting as recombination centers was shown to negatively affect the PDMR detection rate,<sup>[14]</sup> due to the degradation of diamond electronic properties (decrease in the free charge carriers mobility and recombination lifetime).<sup>[20–22]</sup> It has also been demonstrated that the PDMR contrast was limited by the background photocurrent resulting from the photoionization of these defects<sup>[11,14]</sup> and various methods<sup>[12–14]</sup> have been developed to overcome this limitation. We recently reported preliminary results showing that in some diamonds containing NV ensembles, the sign of PDMR resonances—which on most samples appear as a drop in the total green-light induced photocurrent under application of a resonant microwave field—can switch to positive values.<sup>[14]</sup>

Here, we study this intriguing effect of the PDMR resonance sign reversal and propose a mechanism explaining this phenomenon. We first present a detailed experimental investigation of variations in the sign of PDMR resonances. To model this effect we numerically solved Shockley-Read equations for eight electronic levels (related to NV, N<sub>s</sub>, and an additional acceptor defect), including NV spin state sub-levels, and by this way were able to predict the dependence of the PDMR contrast on the incoming laser power. Our study shows that the capture of free electrons by acceptor defects can be responsible for an increase in the hole photocurrent at spin resonance. This increase limits the PDMR contrast and, in some cases, even reverses its sign, as explained below. Acceptor defects with ionization threshold

**Table 1.** Overview of samples used for continuous wave (CW) photoelectric detection of nitrogen-vacancy (NV) magnetic resonance (PDMR) measurements, indicating the method of preparation, the density of NV centers in the sample and the sign of magnetic resonances detected in photocurrent under green illumination.

Sample	Initial sample	Treatment	NV <sup>-</sup> density	Sign of PDMR resonances	Ref.
1	Type-Ib HPHT diamond with [N <sub>s</sub> <sup>0</sup> ] = 200 ppm	Electron-irradiation (14 MeV, 10 <sup>18</sup> cm <sup>-2</sup> ), annealing (700 °C, 4 h)	20 ppm <sup>a)</sup>	Exclusively negative	[11]
2	Type-IIa electronic grade CVD diamond with [N <sub>s</sub> <sup>0</sup> ] < 5 ppb	Implantation of <sup>14</sup> N <sup>4+</sup> ions (8 keV, fluences between 10 <sup>10</sup> and 10 <sup>14</sup> cm <sup>-2</sup> ), annealing (900 °C)	5 to 1000 NVs <sup>b),e)</sup>	Exclusively negative	[12, 13]
3	N-doped CVD diamond	As-grown	[NV <sup>-</sup> ] = 10 ppb <sup>a)</sup>	Exclusively negative	[25]
4	N-doped CVD diamond	Off-angle polishing to form areas with various NV concentrations	Single to a few NVs <sup>c),e)</sup>	Exclusively negative	[17]
5	Electronic grade type-IIa HPHT diamond with [N <sub>s</sub> <sup>0</sup> ] < 5 ppb	As-grown	Single NV centers <sup>d),e)</sup>	Exclusively negative	[17]
6	Type-IIa optical grade CVD diamond with [N <sub>s</sub> <sup>0</sup> ] < 1 ppm	Electron-irradiation (14 MeV, 10 <sup>16</sup> cm <sup>-2</sup> ), annealing (700 °C, 4 h)	10 ppb <sup>a)</sup>	Variable	Full characterization presented in this paper
7	Type-IIa electronic grade CVD diamond with [N <sub>s</sub> <sup>0</sup> ] < 5 ppb	Implantation of <sup>14</sup> N <sup>4+</sup> ions (35 keV, 10 <sup>13</sup> cm <sup>-2</sup> and 60 keV, 10 <sup>13</sup> cm <sup>-2</sup> ), annealing (4 h at 400 °C step, 2 h at 800 °C step and 2 h at 1200 °C)	140 ppb <sup>a)</sup>	Variable	Non-published data
8	N-doped CVD diamond with [N <sub>s</sub> <sup>0</sup> ] = 14 ppm	Electron-irradiation, annealing <sup>a)</sup>	[NV <sup>-</sup> ] = 2 ppm <sup>a)</sup>	Variable	Non-published data
9	N-doped CVD diamond, with [N <sub>s</sub> <sup>0</sup> ] = 50 ppm	Electron-irradiation (16.5 MeV, 8 × 10 <sup>17</sup> cm <sup>-2</sup> ), annealing (700 °C, 45 min and 1000 °C, 90 min) <sup>a)</sup>	[NV <sup>-</sup> ] = 20 ppm <sup>a)</sup>	Variable	Non-published data

<sup>a)</sup> Bulk NV ensembles; <sup>b)</sup> 12 nm-thick NV layer, located approximately 12 nm below the diamond surface; <sup>c)</sup> NV centers within a few nm from the diamond surface; <sup>d)</sup> Isolated single NV centers located ≈2 μm below the diamond surface; <sup>e)</sup> Number of NV centers in focus of the objective, considering 532 nm green laser light focused on the sample using an objective with numerical aperture of 0.95. CVD: chemical vapor deposition. HPHT: high pressure high temperature.

in the near-infrared (NIR) range are shown to be primarily responsible for this phenomenon. We demonstrate that by using a two-color excitation scheme we can selectively photoionize these NIR acceptors, leading to an increase in the spin contrast and in the photoelectric detection rate, and thus to an improvement in the spin detection sensitivity.

## 2. Experimental Characterization of Variations in the Sign of PDMR Resonances

### 2.1. Inversion in the Sign of Photoelectrically Detected Magnetic Resonances

Continuous wave (CW) PDMR experiments consist in detecting the photocurrent resulting from NV centers ionization as a function of the frequency of the microwave field applied to the sample.<sup>[11]</sup> For this, a diamond plate is equipped with coplanar electrodes and green laser light (532 nm) is focused in between electrodes (Figure 1a). The free charge carriers resulting from the two-photon ionization of NV<sup>-</sup> and back conversion from NV<sup>0</sup> to NV<sup>-</sup><sup>[23,24]</sup> are driven toward electrodes by applying a DC electric field, and the resulting photocurrent is detected in an external circuit (see description of experimental setup in Section 6 and further details in Note S1, Supporting Information). As summarized in Table 1, CW-PDMR measurements were performed on a variety of single crystal diamond samples of different origins,

containing NV centers with densities ranging from isolated single defects to highly concentrated NV ensembles.

Further in the text and figures, we refer to a decrease in the photocurrent under application of a spin-resonant microwave field as a negative resonance and to an increase in the photocurrent as a positive resonance. On most samples (samples 1 to 5 in Table 1), PDMR resonances appear as exclusively negative regardless of illumination conditions (light power and depth of light focusing on the sample). Under green illumination, NV<sup>-</sup> triplet ground state <sup>3</sup>A<sub>2</sub> is polarized into the m<sub>s</sub> = 0 spin sublevel. Variations observed in the photocurrent resulting from NV two-photon ionization at resonant microwave frequencies, inducing transitions from the m<sub>s</sub> = 0 to the m<sub>s</sub> = ± 1 spin sublevels of the <sup>3</sup>A<sub>2</sub> state (double-sided arrow on Figure 1b), reflect the spin-dependence of NV<sup>-</sup> photoionization dynamics.<sup>[17,26–28]</sup> Considering the physical mechanisms governing the photoelectric readout of NV spin, discussed in details in various publications previously,<sup>[11,14]</sup> a negative sign is expected for photoelectrically detected magnetic resonances, reflecting the lower ionization rate for electrons in the m<sub>s</sub> = ±1 spin sublevel of NV<sup>-</sup> triplet excited state than for electrons in the m<sub>s</sub> = 0 spin sublevel.

However, on four samples containing bulk NV ensembles (samples 6 to 9 in Table 1)—which were all prepared by high-energy irradiation and annealing of chemical vapor deposited (CVD) diamond crystals—we observed that depending on illumination conditions, the photocurrent either increased or decreased upon application of a resonant microwave field, i.e., showed

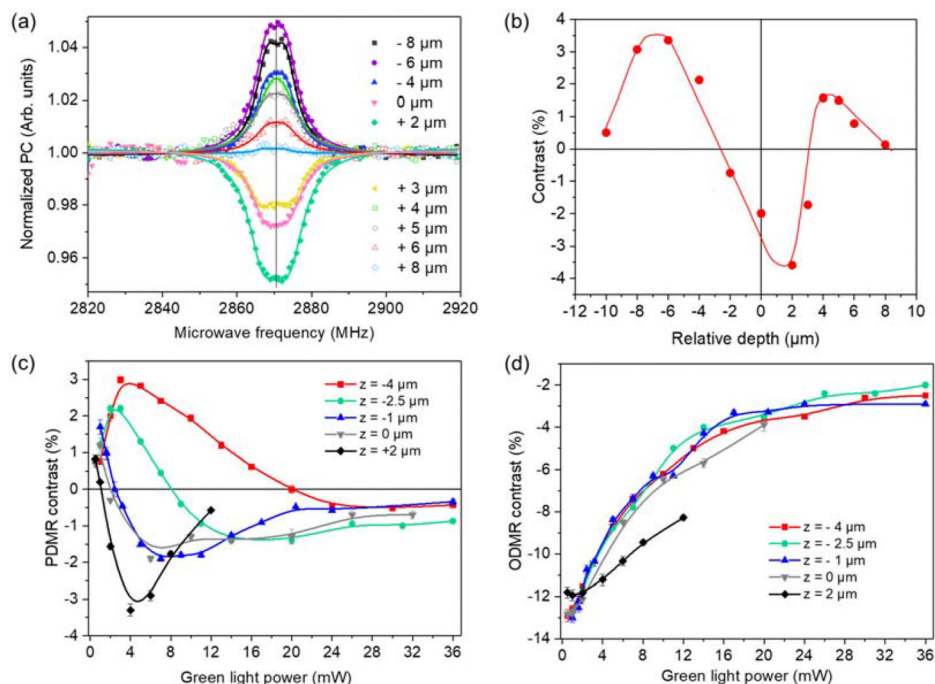


**Figure 2.** a) Positive and negative resonances photoelectrically detected on sample 6 under similar laser and microwave powers, by focusing the laser light at different distances from the diamond surface (green laser power: 7 mW). Symbols: Experimental data. Full lines: fit to the sum of two Lorentzian functions. b) PDMR contrast as a function of the light focusing depth, extracted from the fit of spectra shown in Figure 2a. Scattered points: experimental data. Line: guide for the eye. Simultaneously measured c) PDMR contrasts and d) ODMR contrasts on sample 6 as a function of the green light power, for various light focusing depths. Magnetic resonance contrasts were extracted from the fit of experimental spectra by the sum of two Lorentzian functions. Scattered points: experimental data. Lines: guide for the eye.

either positive or negative spin contrast. It should be mentioned that all samples cited in Table 1 were measured on an identical experimental setup. To completely exclude any measurements artefacts, we performed PDMR and ODMR measurements under an external magnetic field, to induce Zeeman splitting (Figure 1c). The magnetic field-induced Zeeman splitting between the  $m_s = -1$  and  $m_s = +1$  spin sublevels of  $NV^-$  triplet ground state was detected both in PDMR and in the simultaneously measured ODMR spectrum with an identical shape but a different sign, confirming that increases observed in photocurrent reflect indeed  $NV^-$  electron spin resonances. To understand the origin of variations in the sign of PDMR resonances, we performed a detailed study on sample 6, prepared by electron irradiation and annealing of an optical grade type-IIa CVD diamond.

## 2.2. Impact of Green Light Focusing Depth and Power on the Sign of PDMR Resonances

Interestingly, we established that on sample 6 at a constant illumination power, the sign of PDMR resonances varies as a function of the light focusing depth with respect to the diamond surface (Figure 2a,b). At different points on the sample, we observed that the PDMR contrast was positive when the light was focused deep below the surface or far above the surface, while it transitioned to negative values when the focus was moved closer to the diamond surface (negative PDMR obtained for light focusing between  $-2.5$  and  $+3.5$  μm from the surface, where the

indicated depths were measured relatively to the diamond surface, positive values corresponding to a focus above the surface.).

As shown in Figure S1 (Supporting Information) and discussed in Note S2 (Supporting Information), in samples containing bulk ensembles of NV centers the light focusing depth affects the volume of material contributing to the photocurrent signal and consequently the effective light power density in this particular volume. The light power density in the charge collection volume is the highest when light is focused close to the diamond surface and decreases when the focal point is moved away from the sample surface, as confirmed by the depth-dependence of the photocurrent (Figure S2, Supporting Information). These results seem thus to indicate that negative contrasts are observed under high light power density, while lower power densities lead to a positive contrast.

To confirm the influence of the light power density on the sign of resonances, we measured the PDMR contrast as a function of the green light power for various fixed light focusing depths (Figure 2c), and compared it to the simultaneously measured ODMR contrast (Figure 2d). As expected, the ODMR contrast appears to remain negative regardless of the illumination power. The observed decrease in ODMR contrast upon increase of the illumination power results from the rise in the electron spin polarization rate, which exceeds the Rabi frequency under strong illumination.<sup>[29]</sup> The light power-dependence of the ODMR contrast is in addition independent of the focusing depth, except when the light is focused above the diamond surface. The decrease in the absolute value of the negative PDMR contrast ob-



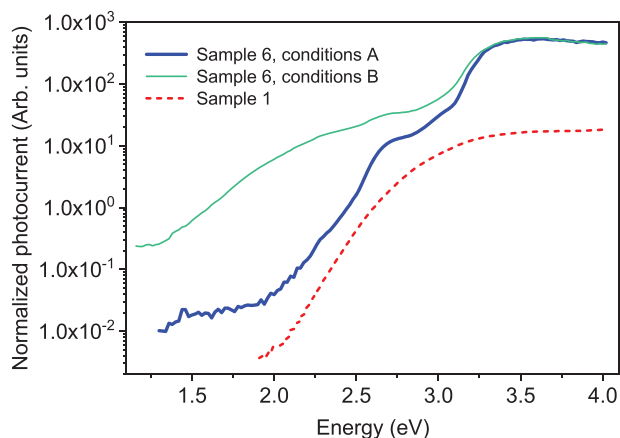


**Figure 3.** Normalized photocurrent spectra measured on sample 6 and sample 1 (excitation:  $0.02$  to  $7 \text{ mW cm}^{-2}$ ). Experimental conditions A: Spectrum measured after leaving the sample in the dark for several days. Experimental conditions B: Spectrum measured just after acquisition of a first spectrum. The relative positions of the two spectra measured on sample 6 are as-measured, while the spectrum measured on sample 1 (acquired in different experimental conditions<sup>[12]</sup> and therefore only presented for a qualitative comparison of the shape of the spectrum) is shifted for clarity.

served under high illumination power can be attributed, like in the case of ODMR, to the excessive light-induced spin polarization rate with respect to the microwave-induced spin transition rate. However, as analyzed in details in Section 3.1.2, the interpretation of variations in the sign of PDMR resonances with the light power requires to consider charge exchanges between NV centers and other optoelectrically active defects in the diamond crystal.

### 2.3. Characterization of the Sample Showing Positive PDMR by Photocurrent Spectroscopy

To gain insight into the optoelectrically active defects present in sample 6, we characterized this sample by photocurrent spectroscopy. For these measurements, the sample was illuminated by monochromatic light, and the photocurrent generated by the ionization of defects was measured as a function of the incident photon energy. It should be emphasized that contrary to PDMR measurements, photocurrent spectroscopy is performed under very low illumination power densities ( $0.02$  to  $7 \text{ mW cm}^{-2}$ , depending on the illumination wavelength), i.e. in conditions for which the one-photon ionization processes dominate over two-photon ones. It does not enable therefore to detect the features associated with the two-photon ionizations of  $\text{NV}^-$  and  $\text{NV}^0$ . Spectra were measured both after leaving the sample in the dark for several days, and just after acquisition of a first spectrum. The spectra acquired on sample 6 were compared to the spectrum measured on sample 1 (electron-irradiated and annealed type-Ib HPHT diamond), on which only negative PDMR resonances were observed (See Figure 3).

On sample 1, a single broad photocurrent band is detected. Fitting of measured data with ab initio calculated ionization cross-sections showed that this spectrum results from a combination of the one-photon ionization bands of neutral substitutional nitrogen ( $\text{N}_s^0$ , photoionization threshold around  $2.2 \text{ eV}$ ),  $\text{NV}^0$  and

$\text{NV}^-$  (one-photon ionization threshold at respectively  $2.78$  and  $2.74 \text{ eV}$ ).<sup>[12]</sup> On sample 6, additionally to the features corresponding to ionization of  $\text{N}_s^0$ ,  $\text{NV}^0$ , and  $\text{NV}^-$  (distinct ionization bands with thresholds around  $2.2$  and  $2.7 \text{ eV}$ ), we observed the presence of other ionization bands in the low-energy and high-energy parts of the spectrum. Note that defects responsible for the two ionization bands with threshold at  $3$  and  $3.2 \text{ eV}$ , i.e., above  $2.33 \text{ eV}$ , cannot contribute to the photocurrent observed in PDMR experiments under green excitation. We further detected an ionization band with onset around  $1.3 \text{ eV}$ , which suggests the existence of defects with ionization threshold in the NIR range, present in higher concentration in sample 6 than in the sample 1 showing exclusively negative PDMR resonances. In the rest of the text, we denote this low-ionization energy defect as X. The explanation for the hysteresis observed in the photocurrent spectrum measured on sample 6 is discussed in Note S4 (Supporting Information).

A full discussion on the nature of defect X and of the defect responsible for the ionization band with threshold at  $3.2 \text{ eV}$  is presented in Section 5.

## 3. Interpretation of Variations in the Sign of PDMR Resonances

### 3.1. Influence of Charge Exchanges between NV and other Defects on the Sign of PDMR Resonances

#### 3.1.1. Origin of Positive PDMR Resonances

A first possible explanation to the formation of positive resonances in the photocurrent could be the detection of electronic transitions from the metastable singlet state  $^1\text{E}$  to the conduction band, as described in references.<sup>[28,30]</sup> These transitions could in theory be induced by green illumination, since it was estimated that the threshold energy for ionization of  $\text{NV}^-$  from the  $^1\text{E}$  level was  $2.2 \pm 0.1 \text{ eV}$ .<sup>[31]</sup> Considering the higher rate of ISC transitions from  $\text{NV}^-$  triplet excited state to the singlet state for electrons prepared in  $m_s = \pm 1$  than for electrons in  $m_s = 0$ , ionization via the metastable state would lead to higher ionization rates at resonance, and therefore to a positive PDMR contrast. However, a theoretical study established that under  $2.33 \text{ eV}$  excitation the cross-section for ionization transitions from  $\text{NV}^-$  triplet excited state  $^3\text{E}$  was more than 10 times higher than the cross-section for ionization from the singlet ground state  $^1\text{E}$ .<sup>[31]</sup> In addition, if ionization from the singlet state was responsible for a significant part of the total photocurrent detected under green illumination, we would expect to observe the formation of positive PDMR resonances on all samples regardless of their composition, while on many samples exclusively negative PDMR resonances were detected (see Section 2.1). The sample-composition dependence of the formation of positive resonances seems to indicate that defects other than NV centers play a role in this phenomenon. In the rest of the discussion we will therefore assume that NV-related photocurrent results in large majority from transitions from the triplet excited state to the conduction band and that the microwave-induced contrast in NV-associated photocurrent can thus only be negative.

In addition to the photocurrent coming from ionization of NV centers, the total detected photocurrent contains a background signal (Figure 4a), partly originating from the ionization of  $\text{N}_s^0$ ,

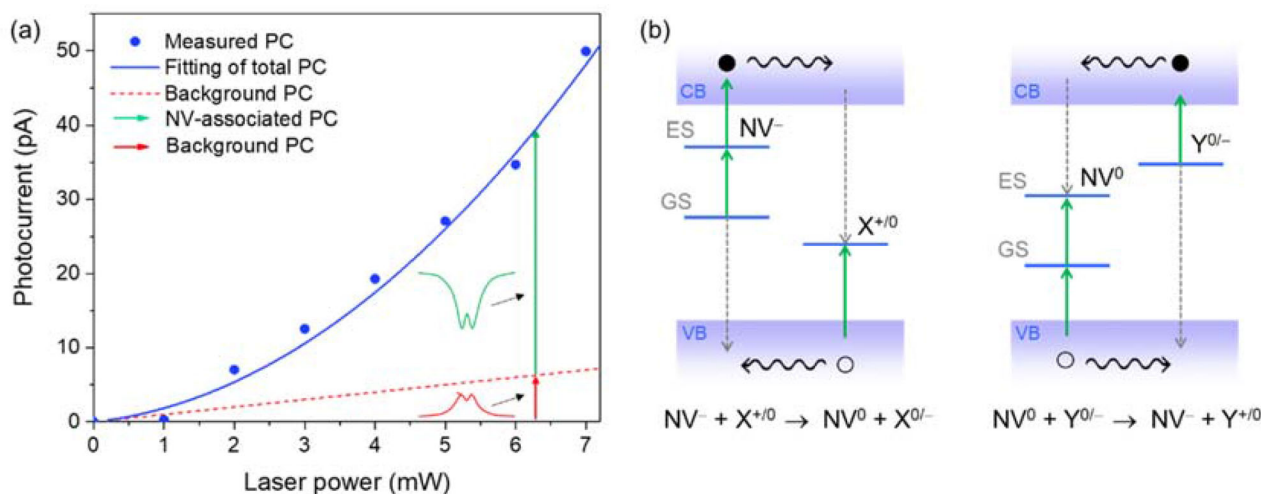


**Figure 4.** a) Schematic representation of the origin of variations in the sign of photoelectrically detected magnetic resonances in the presence of charge exchanges between NV centers and acceptor defects. The green light power dependence of the photocurrent measured 4  $\mu\text{m}$  above the surface of sample 6 was fitted following the method described in Note S5 (Supporting Information), enabling to extract the contribution of the background photocurrent to the total signal. b) Schematic representation of charge exchanges via the conduction or valence band between  $\text{NV}^-$  and an acceptor defect  $\text{X}^{+/0}$  (left) and between  $\text{NV}^0$  and a donor defect  $\text{Y}^{0/-}$  (right).

which is the dominant defect in most samples containing NV centers. As shown by photocurrent spectroscopy, other optoelectrically active defects with ionization threshold below 2.33 eV, acting as electron donors or acceptors, can also contribute to the photocurrent under green illumination. Such background photocurrent has already been shown to limit the PDMR contrast.<sup>[11]</sup> However, this background signal can become spin-dependent if electrons resulting from  $\text{NV}^-$  ionization are captured by acceptor defects. The impact of charge exchanges with donor or acceptor defects on NV charge state has been considered in literature.<sup>[32–37]</sup> Charge exchanges can happen in two steps: first, free charge carriers are formed in the conduction or valence band by the ionization of a defect and in a second step, these free carriers are captured by acceptor or donor centers, respectively (Figure 4b). Charge exchanges between NV and other defects via capture of free charge carriers in the valence or conduction band were for example shown to be responsible for the quenching of photocurrent induced by light pulses under application of a continuous bias light on a sample containing NV ensembles,<sup>[38]</sup> or for the spatial patterns of ionized  $\text{NV}^-$  center formed following red laser illumination.<sup>[39]</sup> It has also been suggested that a direct tunneling of electronic charges from a donor defect to  $\text{NV}^0$  or from  $\text{NV}^-$  to an acceptor defect (representing another possible charge exchange mechanism) can occur in case the average distance between defects is below 5 nm (i.e., in samples presenting an impurity concentration above several tens of ppm).<sup>[40,41]</sup> In sample 6, the concentration of the dominant defect  $\text{N}_s^0$  is below 1 ppm, corresponding to an average distance in between defects above 18 nm, so this tunneling process seems unlikely.

Considering the existence of charge exchanges between  $\text{NV}^-$  and acceptor defects, expressed by the equation shown on the left panel of Figure 4b, the formation of positive resonances can be explained as follows. Under a resonant microwave field,  $\text{NV}^-$  ionization rate is reduced due to the temporary storage of electrons in the metastable state,<sup>[14]</sup> inducing a decrease in NV-associated

photocurrent (Figure 4a). The concentration of free electrons in the conduction band is therefore temporarily lower, leading to a drop in the rate of recombination between free electrons and acceptor defects. In presence of acceptor defects with an ionization threshold below 2.33 eV, the lower rate of recombination between free electrons and acceptor defects results in an augmentation of the one-photon ionization rate of acceptor defects by promotion of an electron from the valence band, and thus to an increase in the hole photocurrent (Figure 4a). The sign of the resonance in the total photocurrent depends therefore on the ratio between NV-related photocurrent and acceptor-related hole photocurrent, determined both by the relative concentrations of these defects in the material and by the light power density.

As mentioned above, photocurrent spectroscopy enabled us to detect in sample 6 the presence of  $\text{N}_s$  and of the defect X, with ionization in the NIR range.  $\text{N}_s$  is the dominant defect in all samples containing NV centers ensembles,<sup>[42–44]</sup> including samples showing exclusively negative resonances. In addition, under green illumination this defect only acts as an electron donor defect, since the light-induced transition from  $\text{N}_s^+$  to  $\text{N}_s^0$  by promotion of an electron from the valence band requires a photon energy higher than 4 eV.<sup>[45]</sup> Based on these two facts, and on the impact of a bias red light on the PDMR contrast (see Section 3.1.3), our hypothesis is that the defect X, detected only in the photocurrent spectrum of the sample presenting variations in the PDMR sign, is the acceptor defect involved in charge exchanges inducing the formation of positive resonances in the photocurrent.

### 3.1.2. Interpretation of Variations in the Sign of PDMR Resonances with the Light Power and Focusing Depth

To check the agreement between the proposed model and the observed light-power dependence of the PDMR contrast, the ratio

between the background photocurrent and NV-related photocurrent was determined as a function of the illumination power and focusing depth, by measuring the green-light power dependence of the photocurrent and by fitting it (Figure S3, Supporting Information, fitting method described in Supporting Information Note S5). The data fitting confirms that the contribution of the background signal to the total photocurrent is higher under low green excitation power, as expected considering the two-photon nature of NV ionization process. For a fixed light power, this contribution also increases with the light focusing distance from the diamond surface. The transition from negative to positive contrasts observed in PDMR when decreasing the green light power (Figure 2c) can thus be explained by the fact that under low power, the background photocurrent (presenting an increase at resonance), dominates over NV-induced photocurrent (showing a decrease at resonance).

It can however be noticed that the absolute value of the PDMR contrast drops under very weak illumination power, while the background photocurrent is still the dominant component of the signal in this range of power. This decrease can be explained by the fact that in these conditions the spin-dependent production of free electrons by ionization of NV<sup>-</sup>, which is a necessary condition to observe microwave-induced variations in the hole photocurrent, becomes too low. The same effect explains the drop in the absolute value of the PDMR contrast observed for a light focusing too far from the diamond surface (Figure 2b), since the effective light power density in the material becomes then very weak.

The potential effect of inhomogeneities in the diamond composition on the depth-dependence of the PDMR contrast is discussed in Note S6 (Supporting Information).

### 3.1.3. Impact of Sub-Resonant Red Bias Illumination on the PDMR Contrast

To experimentally confirm the role of low-ionization energy defects in the alteration of the PDMR sign, we studied the influence of a red bias illumination on the PDMR contrast. For this, sample 6 was illuminated by a combination of CW red light and pulsed green light (Figure 1a). Since the photocurrent is measured by lock-in amplification referenced to the green light pulsing frequency, electronic transitions induced by the red light do not contribute to the detected signal. Red light with a photon energy of 1.88 eV (wavelength of 660 nm) was used. This energy is above the ionization threshold of defect X, but remains below the minimum energy required to excite NV<sup>-</sup> or NV<sup>0</sup> (corresponding to the zero-phonon lines of these defects, at 1.95 and 2.16 eV respectively). After excitation of these defects by a green photon, the absorption of a red photon is however able to induce the second-step of NV<sup>-</sup> ionization or NV<sup>0</sup> recombination.<sup>[27,46,47]</sup>

The PDMR contrast as a function of the red-light power, measured for various fixed green-light powers is presented in Figure 5a. These measurements show that in conditions for which the PDMR contrast is positive under only green illumination, the addition of a red light leads to a transition from positive to negative resonances and to an increase in the absolute value of the PDMR contrast under high red illumination. A contrast of +0.3% under a green illumination of 4 mW could for example

be increased to -3.5% by addition of 10 mW red light. This inversion of the PDMR sign can be explained by the selective ionization of level X. Once filled (i.e., converted to its X<sup>0</sup> form, see Figure 4b), this acceptor defect cannot be ionized by the green light anymore, thus decreasing the contribution of the hole current responsible for the positive resonances to the total signal. The observed impact of red illumination on the PDMR contrast confirms therefore the role of low-ionization energy defects in the inversion of the PDMR resonances sign. In the presence of red light, it can be estimated that the PDMR contrast tends toward the value that it would have in the absence of acceptor defects and measured with the green laser only.

It can be observed that under high red illumination the PDMR contrast saturates and finally decreases. An hypothesis that could explain this phenomenon is that under strong red illumination the rate of NV<sup>-</sup> second ionization step (transition from NV<sup>-</sup> excited state to the conduction band) becomes very high compared to the rate of NV<sup>-</sup> excitation (transition from NV<sup>-</sup> ground to excited state), controlled by the fixed green light power. This could lead to a decrease in the occupation of the  $m_s = \pm 1$  spin sublevel of NV<sup>-</sup> excited state and, therefore, to a diminution in the rate of ISC to the metastable state, resulting in a lower spin contrast in the photocurrent.

The use of a bias red light to improve PDMR performances in terms of contrast and photoelectric detection rate is further described in Section 4.

### 3.2. Modeling of Variations in the Sign of PDMR Resonances

To further verify that the existence of charge exchanges between acceptor defects and NV centers explains the variations observed in the sign of PDMR resonances, we modeled the PDMR process, using the rate model fully described in reference<sup>[48]</sup> (in preparation). For this, we considered light-induced and recombination transitions associated with NV center, substitutional nitrogen N<sub>S</sub> and the acceptor defect X, as described in Figure 5b (more details, including the ionization and recombination rates used for modeling are given in Note S7 and Table S1, Supporting Information). Under green illumination the following four photo-ionization processes were considered:



We used a 1D model in which the different point defects are distributed in 11 cells, and the flux of charge carriers in between the different cells due to their drift in the external electric field is considered, as detailed in Supporting Information. To take into account the excess of N<sub>S</sub> defects in the sample 6 under study, each of the 11 cells contains a N<sub>S</sub> center, while only the central cell contains a NV center. To study the influence of acceptor defects on the PDMR contrast, a number of acceptor defects X between 0 and 7 was also distributed in the different cells. It has to be emphasized that this 1D rate modeling of a small number of defects

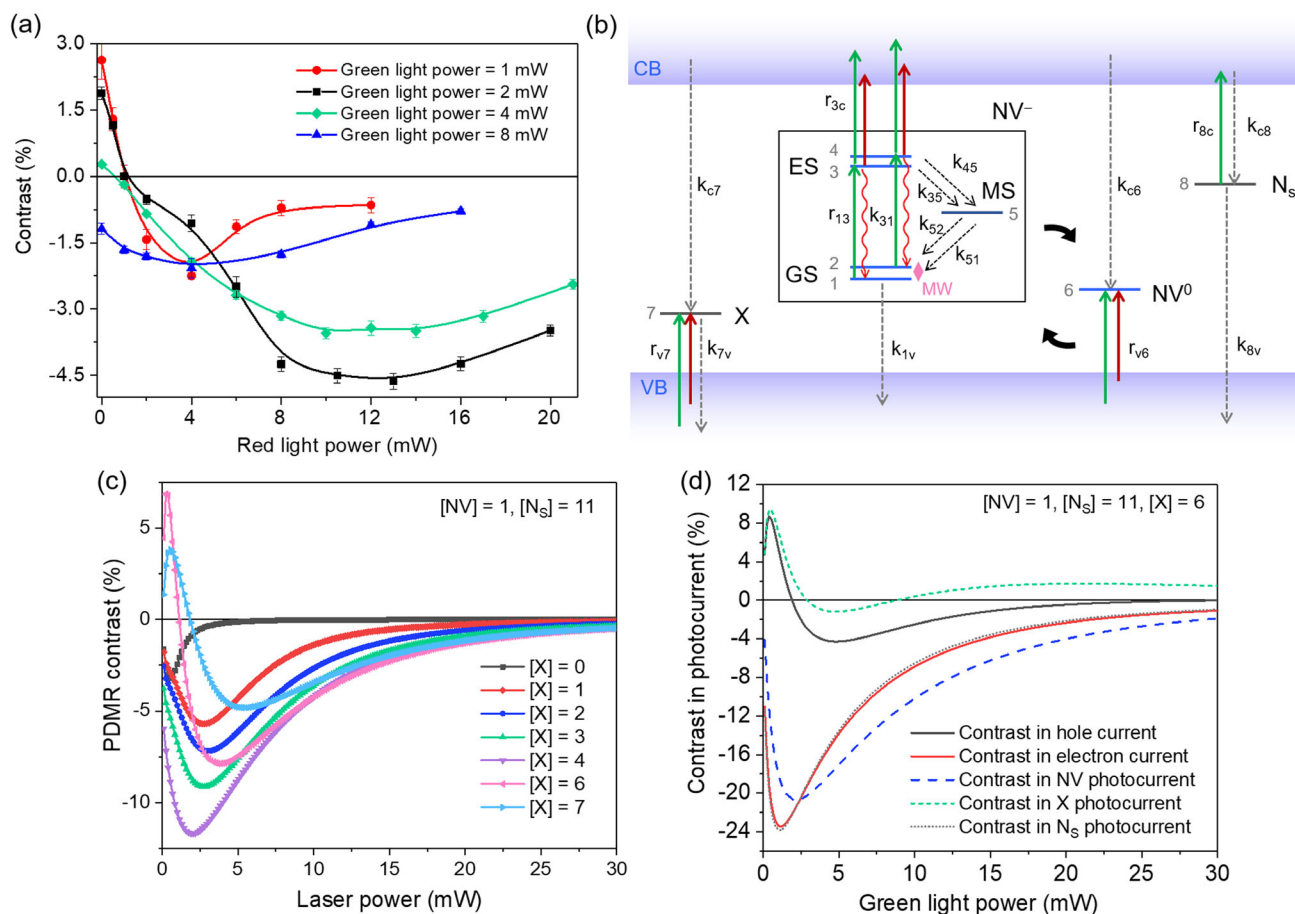


**Figure 5.** a) Photoelectrically detected magnetic resonance contrast obtained on sample 6 under combined pulsed green (2.33 eV) and continuous wave (CW) red (1.88 eV) bias illumination. Light focusing 2  $\mu\text{m}$  below the diamond surface. Symbols: experimental data. Lines: guide for the eye. The data presented in this figure were not recorded at the same point on the sample as the data shown on Figure 2, explaining why the PDMR contrasts appearing in the two figures slightly differ. b) Schematic representation of electronic levels and transitions considered to model variations in the sign of PDMR resonances. Full green and red arrows: transitions induced by respectively green (532 nm) and red (660 nm) light, exciting an electron from the valence band to an empty defect level, from an occupied defect level to the conduction band or from NV<sup>-</sup> triplet ground state (GS) to its triplet excited state (ES). Wavy red arrows: spin-conserving photoluminescent transitions between the triplet ES and GS of NV<sup>-</sup>. Dashed black arrows: nonradiative ISC transitions between NV<sup>-</sup> triplet states and singlet metastable states (MS). Dashed grey arrows: nonradiative recombination between an electron in the conduction band and an empty defect level, or between an occupied defect level and a hole.  $k_{ij}$ : rate of recombination from level  $i$  to level  $j$  (indexes c and v are used to note the conduction and valence bands, respectively), in Hz.  $r_{ij}$ : rate of light-induced transitions from level  $i$  to level  $j$  (in Hz  $\text{mW}^{-1}$ ). c) Calculated green-light power dependence of the PDMR contrast, for different numbers of acceptor defects X. [X]: number of defect X, considering 1 NV center and 11 N<sub>s</sub> defects. d) In the case [X] = 6, calculated MW-induced contrast in the total hole photocurrent, the total electron photocurrent, as well as in the photocurrent associated with N<sub>s</sub>, X, and NV ionization.

can only be used for a qualitative comparison with experimental data, which were acquired on a large ensemble of bulk defects.

Calculations performed using this model first show that when only NV and N<sub>s</sub><sup>0</sup> are present ([X] = 0 in Figure 5c), the magnetic resonances formed in the photocurrent are always negative, regardless of the green-light power applied or of the value considered for the different recombination rates. Indeed, as expected, the photocurrent calculated considering only the free charge carriers resulting from NV<sup>-</sup> and NV<sup>0</sup> ionization systematically decreases under application of a resonant microwave field (i.e., presents a negative resonance) (see Figure S4, Supporting Information). In the absence of defect X, the photocurrent calculated considering only the free electrons resulting from N<sub>s</sub><sup>0</sup> ionization also shows a small negative microwave-induced reso-

nance (up to  $-2.6\%$ ) (Figure S4, Supporting Information). This resonance in N<sub>s</sub><sup>0</sup>-associated photocurrent is due to the fact that under a resonant microwave field, the reduction in the amount of free charge carriers resulting from NV<sup>-</sup> ionization induces a decrease in the rate of electron capture by N<sub>s</sub><sup>+</sup> and thus a decrease in the rate of N<sub>s</sub><sup>0</sup> ionization (given that the capture of an electron by N<sub>s</sub><sup>+</sup> leads to the formation of N<sub>s</sub><sup>0</sup>). This negative contrast in N<sub>s</sub><sup>0</sup>-photocurrent is well smaller than the negative contrast in NV-associated photocurrent (up to  $-20\%$ ). The modeling results confirm thus that the presence of N<sub>s</sub> defects in large excess leads to a limitation of the total PDMR contrast (negative PDMR contrast of maximum  $-2.6\%$  observed in the case [X] = 0), in good agreement with experimental observations.<sup>[14]</sup>



The formation of positive resonances requires to introduce an acceptor level in the mathematical model, and to consider that the positively charged state of this defect ( $X^+$ ) presents a large electron capture cross-section (considered 20 times higher than the electron capture cross-section of  $N_S^+$  to obtain the data presented in Figure 5). It can be observed in Figure 5c that the introduction of a small amount (1 to 4) of acceptor defect  $X$  in the model leads to an increase in the absolute value of the negative PDMR contrast. Indeed, the recombination of free electrons with  $X^+$  (considered to have a large capture cross-section) competes with their recombination with  $N_S^+$ , further reducing the reformation of  $N_S^0$  and thus decreasing the photocurrent associated with  $N_S^0$  ionization. This leads to an increase in the absolute value of the negative contrast in  $N_S^0$ -photocurrent (up to  $-11.3\%$  for  $[X] = 4$ ). Due to the higher number of  $N_S$  defects, in the range  $[X] = 1$  to  $[X] = 4$ ,  $N_S$ -associated photocurrent dominates over  $X$ -associated photocurrent, and the overall PDMR contrast remains negative in the whole range of excitation power.

If a sufficient number of defect  $X$  is introduced into the mathematical model ( $[X] \geq 6$  in Figure 5c), the calculated green-light power dependence of the PDMR contrast appears qualitatively similar to the experimentally observed dependence (transition from negative to positive contrast upon reduction of the illumination power, followed by a slight decrease of the positive contrast when the illumination power approaches zero—see Figure 2c). In the case  $[X] = 6$ , calculations of the microwave-induced spin contrast (Figure 5d) indicate that the photocurrent resulting from  $NV^-$  and  $NV^0$  ionization decreases at resonance (negative contrast up to  $-20\%$ ).  $N_S^0$ -associated photocurrent also presents a large negative contrast (up to  $-22\%$ ), resulting as explained above from charge exchanges between  $NV^-$  and  $N_S^+$ . The microwave-induced contrast in the electron photocurrent (resulting from  $NV^-$  and  $N_S^0$  ionization) is therefore always negative. On the contrary, under low illumination the photocurrent associated with  $X^+$  ionization increases at resonance, as expected considering the capture of free electrons resulting from  $NV^-$  ionization by this defect (see Section 3.1). In case the concentration of defect  $X$  with respect to  $NV$  and  $N_S$  is sufficient, this causes an augmentation of the hole photocurrent at resonance, and ultimately leads to the positive contrast observed in the total photocurrent under low-power green illumination.

These modeling results therefore clearly suggest that in presence of acceptor defects, the hole photocurrent limits the PDMR contrast, and in some particular conditions, can lead to an inversion in the sign of PDMR resonances.

## 4. Optimization of PDMR Performances by Selective Ionization of Low Energy Acceptor Defects

### 4.1. Influence of Red Bias Illumination on the PDMR Sensitivity in the Case of a Sample Showing Variations in the Sign of PDMR Resonances

In this section, we demonstrate how the addition of a red bias light with photon energy of 1.88 eV (i.e., below  $NV^-$  excitation threshold) can be used to enhance the PDMR performance and thus improve the sensitivity of PDMR sensors based on NV ensembles.

The shot-noise limited sensitivity of NV diamond sensors based on the CW detection of NV magnetic resonances can be expressed as:

$$\eta = \frac{4h}{3\sqrt{3}g\mu_B} \frac{\Delta\nu}{C\sqrt{R}} \quad (5)$$

where  $h$  is the Planck constant,  $g$  is NV gyromagnetic ratio,  $\mu_B$  is the Bohr magneton,  $C$  is the magnetic resonance contrast,  $\Delta\nu$  the magnetic resonance full-width-half-maximum, and  $R$  the photon (for ODMR) or charge carrier (for PDMR) detection rates.<sup>[19]</sup>

Experimental characterizations have shown that on some samples containing NV ensembles, addition of a red bias light with an energy below  $NV^-$  excitation threshold could be used to selectively ionize NIR acceptor defects and thus increase the absolute value of the PDMR contrast (Section 3.1.3). At a fixed green-light power, application of red bias light also causes an increase in the green-light induced photocurrent measured on sample 6 (Figure 6a). Application of bias red light with a power of 20 mW enables for example to increase the photocurrent by a factor 2.2 under 8 mW green illumination and by a factor 13.7 under 1 mW green illumination. The explanation for this increase in photocurrent under red illumination is discussed in Note S8 (Supporting Information).

Further on, the PDMR sensitivity obtained on sample 6 by varying the red-light power for various fixed green-light powers was compared to the sensitivity obtained by performing PDMR and ODMR under only green illumination on the same sample (Figure 6b).

It can be noted that under only green illumination the optimal PDMR sensitivity is approximately 20% better than the optimal ODMR sensitivity, in spite of the lower contrasts observed in PDMR (see Figure 2c,d). This better sensitivity results from the higher detection rates enabled by the photoelectric detection on this sample (see Figure S5, Supporting Information, and Note S9, Supporting Information), in accordance with findings in.<sup>[12,14,17]</sup> However, the improvement in sensitivity enabled by the use of PDMR remains rather low here, due to the fact that the photoelectric detection rate becomes significantly higher than the photoluminescence rate in conditions for which both the PDMR and ODMR contrasts are low (i.e., under strong illumination).

Under low green illumination, the PDMR contrast is positive in the absence of red bias light. The addition of a weak red bias light under a fixed green power initially induces a decrease in the positive PDMR contrast, explaining the degradation of the sensitivity observed in the first part of the curves. However, for red-light powers higher than the value leading to an annulation of the PDMR contrast, the contrast becomes negative and its absolute value increases with the red-light power, leading to an improvement in the sensitivity. At a given green illumination power, addition a red light leads thus to a strong improvement of the PDMR sensitivity (e.g., an improvement of the sensitivity of a factor 11.5 is obtained by adding 18 mW red light to a 4 mW green light).

A combination of red and green light enables PDMR to clearly exceed the ODMR sensitivity on this sample. In these conditions, the optimal PDMR sensitivity (obtained under 4 mW green and 14 mW red) is improved by a factor 1.8 compared to the best PDMR sensitivity obtained under only green illumination (20 mW) and by a factor 2.1 compared to the best ODMR

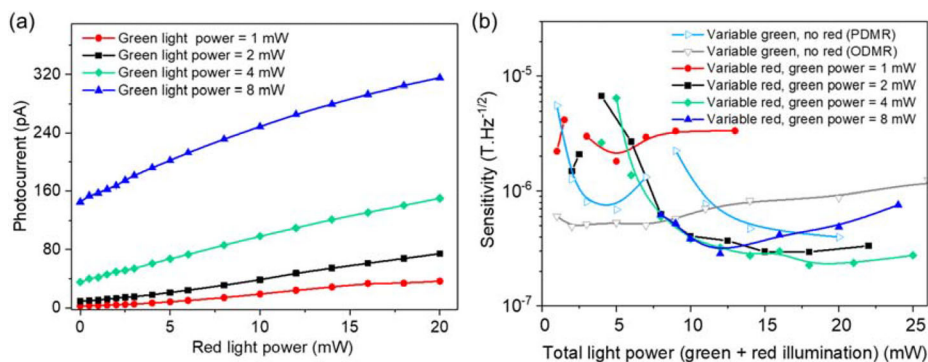


**Figure 6.** a) Influence of the red bias light power on photocurrent measured on sample 6 under combined pulsed green (2.33 eV) and continuous wave (CW) red (1.88 eV) bias illumination, for various fixed green light powers. Light focusing 2  $\mu\text{m}$  below the diamond surface. Symbols: experimental data. Lines: guide for the eye. b) Full symbols: sensitivity obtained by performing photoelectric detection of nitrogen-vacancy (NV) magnetic resonance (PDMR) measurements under combined pulsed green light and CW red bias light. Empty symbols: sensitivity obtained by performing optical detection of magnetic resonance (ODMR) and PDMR measurements under green illumination only, presented for comparison. Data are represented as a function of the total illumination power (sum of the red and green light power). Symbols: experimental data. Lines: guide for the eye. Interruptions in the curves correspond to values of the light power for which the PDMR contrast is zero.

sensitivity. It has to be underlined that the best PDMR sensitivity obtained here ( $\approx 200 \text{ nT } \sqrt{\text{Hz}^{-1}}$ ) remains rather high compared to results reported in literature on NV ensembles. Indeed, the sample 6 used here to study the role of acceptor defects on PDMR presents a very broad FWHM at resonance (linewidth of  $\approx 9 \text{ MHz}$ ) and thus do not have by far optimal properties for magnetometry. However, our technique can be applied on samples presenting better characteristics for diamond magnetometry (e.g.,  $^{12}\text{C}$  enriched samples showing very narrow resonances), and could lead to interesting gains in terms of magnetic field sensitivity. Recently, we have characterized irradiated CVD samples containing 2 ppm of NV centers and presenting a FWHM of  $\approx 100 \text{ kHz}$  (mentioned as sample 8 in Table 1), on which we detected a positive PDMR contrast [paper in preparation].

#### 4.2. Influence of Red Bias Illumination on the PDMR Sensitivity in the Case of an Irradiated Sample Showing only Negative Resonances

Even when the concentration of acceptor defects in a sample is not sufficient to induce the switching of the PDMR resonance sign, their presence should lead to a reduction in the absolute value of the contrast which can consequently be improved by using the two-color excitation method. To test this hypothesis, we studied the effect of an additional subresonant red bias light on PDMR measurements performed on an irradiated nitrogen-rich HPHT diamond (sample 1). Indeed, similarly to sample 6 this sample was submitted to electron-irradiation and annealing. Some of the defects present in sample 6—in particular irradiation-induced defects—are thus likely to be also present in sample 1.

On sample 1 we observed that under green illumination, the PDMR contrast always remained negative, and presented values below 1%, i.e., approximately 8.5 times lower than the maximal ODMR contrast observed on the same sample (see Figure S6, Supporting Information, and Note S10, Supporting Information). The addition of red light under fixed green light power appears to enhance the PDMR contrast (Figure 7a), up to a factor

4.5 in case of low green illumination (0.4–2 mW) combined with a strong red bias light ( $>10 \text{ mW}$ ). As shown in Figure 7b, under constant total illumination power (sum of the green- and red-light powers), replacing a fraction of the green light by red light leads to a significant increase in the PDMR contrast (under a total power of 12 mW, contrast increased by a factor 4.5 by using a combination of 11 mW red and 1 mW green instead of only green light). Like on sample 6, an increase in the green-light induced photocurrent is observed upon addition of a red bias light (Figure S7a, Supporting Information), leading to an improvement of the PDMR sensitivity on this sample (See Figure S7b, Supporting Information, Note S11, Supporting Information). These results confirm thus the limitation of the PDMR contrast by the presence low ionization energy defects, even on samples on which the PDMR resonances always appear negative.

### 5. Discussion on the Nature of Low-Ionization Energy Defects Involved in Charge Exchanges with NV Centers

Here we discuss the possible nature of the low-ionization energy X-defect. Photoionization bands with a threshold at 1.3 eV or lower were previously reported on intrinsic<sup>[49]</sup> or N-doped<sup>[50,51]</sup> CVD diamond. Based on the influence of surface oxidation or hydrogenation on the amplitude of this ionization band, it was attributed to the ionization of a hydrogen-related acceptor defect located at the diamond surface.<sup>[51]</sup> However, PDMR measurements were here performed on an oxidized sample. Oxidation very effectively removes H-termination, which would also quench NV-photoluminescence. Our experiments were in addition performed on a sample containing bulk NV ensembles, using electrodes separated by a large distance (15  $\mu\text{m}$ ) and enabling therefore the collection of electric charges from deep inside the diamond (see Note S2, Supporting Information). It is therefore unlikely that H-related surface defects are responsible for the observed variations in the PDMR sign.

The four diamond samples showing variations in the sign of PDMR resonances (samples 6 to 9 in Table 1), as well as the

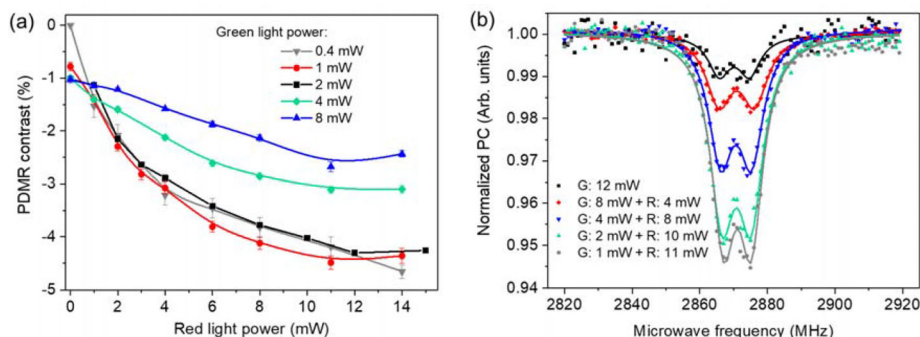


**Figure 7.** a) Red-light power dependence of the photoelectrically detected magnetic resonance contrast measured on sample 1 under combined pulsed green excitation (2.33 eV) and continuous wave (CW) red bias illumination (1.88 eV), for various fixed green light powers. Measurements performed at the surface level. Symbols: experimental data. Lines: guide for the eye. b) Comparison between PDMR spectra measured under a similar total illumination power of 12 mW, using only green light or a combination of pulsed green light and CW red bias light. Symbols: experimental data. Lines: fit to the sum of two Lorentzian functions.

sample on which an increase in the absolute value of the PDMR contrast could be obtained under a red bias illumination (sample 1, see Section 4.2) were all submitted to irradiation by high energy particles (nitrogen ions or electrons) and annealed. This observation seems to indicate that X-defects are introduced in the diamond crystal by irradiation, and could thus correspond to interstitial atoms or vacancy-related defects.<sup>[52]</sup> Defects formed by the combination of vacancies with nitrogen aggregates (and in particular the H3 optical center, corresponding to the N-V-N structure) are mostly found in irradiated and annealed natural diamond, or in diamond annealed above 2000 °C.<sup>[53,54]</sup> These defects are therefore probably not present in significant concentration in the irradiated CVD sample on which we observed variations in the sign of PDMR resonances (sample 6).

NVH was reported to be present in as-grown CVD diamond,<sup>[55]</sup> with a concentration approximately 30 times higher than NV.<sup>[43]</sup> Two bands with thresholds around 1.1 and 2.2 eV were detected in the optical absorption spectra of CVD diamond and attributed to the ionization of this defect.<sup>[42]</sup> It has however to be stressed that Khan et al. ascribed the band with the lowest ionization energy (threshold around 1.1 eV) to the ionization of NVH<sup>-</sup>, acting as a donor defect. They associated the ionization of the acceptor form of the defect, NVH<sup>0</sup>, to a band with onset at 2.2 eV (which would therefore be undistinguishable from N<sub>s</sub><sup>0</sup> ionization band, due to the very close photoionization thresholds of these two defects). NVH could in principle be the defect involved in charge exchanges with NV and responsible for the formation of positive PDMR resonances. However, following the findings of Khan et al., the red bias light (with an energy of 1.88 eV, i.e., below the ionization threshold they attribute to NVH<sup>0</sup>) would not be able to ionize the NVH<sup>0</sup> level, which contradicts the effect of the red bias light on the PDMR contrast observed in our experiments (see Section 3.1.3). In addition, we showed that the limitation of the absolute value of the PDMR contrast by the increase in the hole photocurrent at resonances also existed on an irradiated type-Ib HPHT sample (see Section 4.2), while the NVH defect is usually not observed in this type of samples, suggesting that other defects are involved in charge exchanges with NV centers.

Ab initio calculations predicted that the single vacancy V presented transitions between the positive and neutral charge states 1 eV above the valence band, and between the neutral and neg-

ative charge states 2.1 eV above the valence band.<sup>[53]</sup> These transitions could thus correspond to the ionization bands that we observed by photocurrent spectroscopy on sample 6. For the divacancy V<sub>2</sub>, the transition between the positive and neutral charge states was calculated to be located 1.2 eV above the valence band, and between the neutral and negative charged states 2.4 eV above the valence band.<sup>[53]</sup> An experimental study of the electronic properties of electron-irradiated high-purity CVD diamonds showed in addition that irradiation leads to a strong drop in the lifetime of free charge carriers, due to their fast recombination with vacancy-associated defects.<sup>[22]</sup> Photoluminescence and optical absorption measurements performed on these irradiated samples after annealing at various temperatures enabled to demonstrate that the dominant recombination center was the single vacancy for samples annealed below 900 °C and the divacancy for samples annealed between 900 °C and 1000 °C.<sup>[22]</sup> It was in addition established that the neutral single vacancy presented a high capture cross-section (6.3 × 10<sup>-16</sup> cm<sup>2</sup>, versus 1 × 10<sup>-16</sup> cm<sup>2</sup> for N<sub>s</sub><sup>0</sup>). Considering that sample 6 used in our study was annealed at 700 °C, the recombination of charge carriers with the single vacancy is the most likely. The transition from V<sup>+</sup> to V<sup>0</sup> by promotion of an electron from the valence band would in this case account for the NIR ionization band we observed in photocurrent spectroscopy:



Since theoretical calculations<sup>[53]</sup> indicate that the ground state of V<sup>0</sup> is located approximately 2.1 eV above the valence band, the ionization band with threshold around 3.2 eV observed in the photocurrent spectrum of sample 6 could in this case correspond to the opposite photoionization process, in which V<sup>0</sup> is converted to V<sup>+</sup> by promotion of an electron to the conduction band:



This transition would explain the hysteresis observed in photocurrent spectroscopy measurements, in which following illumination of the sample with high energy photons, the intensity of the NIR band corresponding to V<sup>+</sup> ionization is seen to strongly increase (see Note S4, Supporting Information).

It should be emphasized that the interpretation we propose requires to consider that the positively charged single vacancy  $V^+$  is present in significant concentration in the sample 6 under study. It has also to be noted that the ZPL associated with  $V^0$  (or GR1 center, at 741 nm) was not detected in the photoluminescence spectrum measured on sample 6 (Figure S8, Supporting Information, Note S12, Supporting Information), on which only the characteristic features of  $NV^-$  and  $NV^0$  were observed. This could be explained by the fact that we used for these measurements a relatively strong excitation at a wavelength of 532 nm, corresponding to a photon energy of 2.33 eV, i.e., above the threshold for the transition from  $V^0$  to  $V^-$  by promotion of an electron from the valence band.<sup>[53]</sup>

## 6. Conclusion

In conclusion, we reported an interesting phenomenon, the switch in the sign of photoelectrically detected NV electron spin resonance from negative to positive. Based on a detailed experimental study and mathematical modeling, we developed a model enabling to explain the formation of positive PDMR resonances. We have in particular shown that charge exchanges between NV centers and other optoelectrically active defects strongly impacted the photoelectric readout of NV spin. We have demonstrated that in case charge exchanges occurred between NV and acceptor defects in diamond, the hole photocurrent related to the ionization of acceptors could increase under application of a resonant microwave field. This phenomenon can limit the PDMR contrast and lead, depending on the sample composition and on illumination conditions, to an inversion in the sign of PDMR resonances. In electron-irradiated CVD diamond, acceptor defects with ionization energy in the NIR region (thought to be single vacancies) were found to be primarily involved in charge exchanges with NV centers and therefore responsible for the formation of positive PDMR resonances. This study has thus proved the importance of carefully tuning the diamond composition to optimize the PDMR performances and develop high-sensitivity photoelectrically readout diamond quantum sensors.

We have also shown on two different samples that application of a red bias light with photon energy below  $NV^-$  excitation threshold, to selectively ionize low energy acceptor defects, led to increases in the absolute value of the PDMR contrast and in the photoelectric detection rate. On an irradiated optical-grade type-IIa CVD diamond, application of this bias light enabled to reach a PDMR sensitivity exceeding the ODMR sensitivity by a factor 2. This method is particularly relevant to enhance the sensitivity of PDMR sensors based on NV ensembles. Beyond optimization of PDMR performances, studying charge exchanges between NV centers and other defects is essential, since these exchanges have been demonstrated to affect the charge stability of  $NV^-$  centers—especially in case of shallow implanted defects<sup>[36,37]</sup>—which is critical for all quantum applications of NV centers.<sup>[2]</sup>

## 7. Experimental Section

**Samples Preparation:** The samples 6 and 1 used in the experimental study were prepared by electron irradiation and annealing of optical grade 111-oriented type-IIa CVD diamond and of 100-oriented type-Ib HPHT diamond, respectively (see composition of the samples and preparation con-

ditions in Table 1). Coplanar Ti-Al interdigitated electrodes separated by a gap of 15  $\mu\text{m}$  were fabricated on one of the faces of the diamond plates, using optical lift-off lithography and metal sputtering. More details on the sample preparation are presented in Note S1 (Supporting Information).

**Experimental Setup:** For ODMR and PDMR measurements, the samples were placed on a home-built confocal photoluminescence microscope equipped with pulsed green (532 nm, Nd-YAG laser) and CW red (660 nm, laser diode) light sources and enabling illumination of the sample by one or a combination of these wavelengths. The laser light was focused onto the diamond using an air objective with numerical aperture of 0.95. After pre-amplification using a low-noise current-to-voltage pre-amplifier (gain of 2  $\text{nA V}^{-1}$ ), the photocurrent was detected by lock-in amplification (time constant: 100 ms) referenced to the green light pulsing frequency (131 Hz). The power of the microwave field (applied using a Cu wire with 50  $\mu\text{m}$  diameter pressed against the diamond surface) and the magnitude of the bias electric field applied in between electrodes (5  $\text{V } \mu\text{m}^{-1}$  on sample 1, 3.3  $\text{V } \mu\text{m}^{-1}$  on sample 6) were kept constant, since it was observed that these parameters did not affect the sign of PDMR resonances. In case of pulsed illumination, the power mentioned in the graphs and text is the peak power during the on-period of the signal, and not the effective power averaged in time. More details on experimental setups are provided in Note S1 (Supporting Information).

## Supporting Information

Supporting Information is available from the Wiley Online Library or from the author.

## Acknowledgements

This work was supported by the Grant Agency of the Czech Republic (Project Number 16–163365), the FWO project DIAQUANT (S004018N), the FWO Project G0E7417N, the QUANTERA project Q-Magine (R-8843), and the EU project ASTERIQS (820394). The authors thank D. Budker and A. Jarmola for providing some of the samples used in this study.

## Conflict of Interest

The authors declare no conflict of interest.

## Data Availability Statement

The data that support the findings of this study are available from the corresponding author upon reasonable request.

## Keywords

crystal defects in diamond, charge exchanges, electron spin resonances, nitrogen-vacancy centers, photoelectric detection

Received: December 1, 2021  
Published online: March 17, 2022

- [1] L. Rondin, J. P. Tetienne, T. Hingant, J. F. Roch, P. Maletinsky, V. Jacques, *Rep. Prog. Phys.* **2014**, *77*, 056503.
- [2] J. F. Barry, J. M. Schloss, E. Bauch, M. J. Turner, C. A. Hart, L. M. Pham, R. L. Walsworth, *Rev. Mod. Phys.* **2020**, *92*, 015004.
- [3] F. Dolde, H. Fedder, M. W. Doherty, T. Nöbauer, F. Rempp, G. Balasubramanian, T. Wolf, F. Reinhard, L. C. L. Hollenberg, F. Jelezko, J. Wrachtrup, *Nat. Phys.* **2011**, *7*, 459.



- [4] E. H. Chen, H. A. Clevenson, K. A. Johnson, L. M. Pham, D. R. Englund, P. R. Hemmer, D. A. Braje, *Phys. Rev. A* **2017**, *95*, 053417.
- [5] G. Kucsko, P. C. Maurer, N. Y. Yao, M. Kubo, H. J. Noh, P. K. Lo, H. Park, M. D. Lukin, *Nature* **2013**, *500*, 54.
- [6] P. Neumann, I. Jakobi, F. Dolde, C. Burk, R. Reuter, G. Waldherr, J. Honert, T. Wolf, A. Brunner, J. H. Shim, D. Suter, H. Sumiya, J. Isoya, J. Wrachtrup, *Nano Lett.* **2013**, *13*, 2738.
- [7] B. Grotz, J. Beck, P. Neumann, B. Naydenov, R. Reuter, F. Reinhard, F. Jelezko, J. Wrachtrup, D. Schweinfurth, B. Sarkar, P. Hemmer, *New J. Phys.* **2011**, *13*, 055004.
- [8] F. Shi, Q. Zhang, P. Wang, H. Sun, J. Wang, X. Rong, M. Chen, C. Ju, F. Reinhard, H. Chen, J. Wrachtrup, J. Wang, J. Du, *Science* **2015**, *347*, 1135.
- [9] H. J. Mamin, M. Kim, M. H. Sherwood, C. T. Rettner, K. Ohno, D. D. Awschalom, D. Rugar, *Science* **2013**, *339*, 557.
- [10] T. Wolf, P. Neumann, K. Nakamura, H. Sumiya, T. Ohshima, J. Isoya, J. Wrachtrup, *Phys. Rev. X* **2015**, *5*, 041001.
- [11] E. Bourgeois, A. Jarmola, P. Siyushev, M. Gulka, J. Hruby, F. Jelezko, D. Budker, M. Nesladek, *Nat. Commun.* **2015**, *6*, 8577.
- [12] E. Bourgeois, E. Londero, K. Buczak, J. Hruby, M. Gulka, Y. Balasubramaniam, G. Wachter, J. Stursa, K. Dobes, F. Aumayr, M. Trupke, A. Gali, M. Nesladek, *Phys. Rev. B* **2017**, *95*, 041402(R).
- [13] M. Gulka, E. Bourgeois, J. Hruby, P. Siyushev, G. Wachter, F. Aumayr, P. R. Hemmer, A. Gali, F. Jelezko, M. Trupke, M. Nesladek, *Phys. Rev. Appl.* **2017**, *7*, 044032.
- [14] E. Bourgeois, M. Gulka, M. Nesladek, *Adv. Opt. Mater.* **2020**, 1902132.
- [15] F. M. Hrubesch, G. Braunbeck, M. Stutzmann, F. Reinhard, M. S. Brandt, *Phys. Rev. Lett.* **2017**, *118*, 037601.
- [16] T. Murooka, M. Shiigai, Y. Hironaka, T. Tsuji, B. Yang, T. M. Hoang, K. Suda, K. Mizuno, H. Kato, T. Makino, M. Ogura, S. Yamasaki, M. Hatano, T. Iwasaki, *Appl. Phys. Lett.* **2021**, *118*, 253502.
- [17] P. Siyushev, M. Nesladek, E. Bourgeois, M. Gulka, J. Hruby, T. Yamamoto, M. Trupke, T. Teraji, J. Isoya, F. Jelezko, *Science* **2019**, *363*, 728.
- [18] M. Gulka, D. Wirtitsch, V. Ivády, J. Vodnik, J. Hruby, G. Magchiels, E. Bourgeois, A. Gali, M. Trupke, M. Nesladek, *Nat. Commun.* **2021**, *12*, 4421.
- [19] A. Dréau, M. Lesik, L. Rondin, P. Spinicelli, O. Arcizet, J.-F. Roch, V. Jacques, *Phys. Rev. B* **2011**, *84*, 195204.
- [20] T. Malinauskas, K. Jarasiunas, E. Ivakin, V. Ralchenko, A. Gontar, S. Ivakhnenko, *Diamond Relat. Mater.* **2008**, *17*, 1212.
- [21] P. Ščajev, V. Gudelis, E. Ivakin, K. Jarašiunas, *Phys. Status Solidi* **2011**, *208*, 2067.
- [22] P. Grivickas, P. Ščajev, N. Kazuchits, S. Lastovskii, L. F. Voss, A. M. Conway, A. Mazanik, O. Korolik, V. Bikbajevs, V. Grivickas, *Appl. Phys. Lett.* **2020**, *117*, 242103.
- [23] N. Aslam, G. Waldherr, P. Neumann, F. Jelezko, J. Wrachtrup, *New J. Phys.* **2013**, *15*, 013064.
- [24] P. Siyushev, H. Pinto, M. Vörös, A. Gali, F. Jelezko, J. Wrachtrup, *Phys. Rev. Lett.* **2013**, *110*, 167402.
- [25] E. Bourgeois, M. Gulka, D. Wirtitsch, P. Siyushev, H. Zheng, J. Hruby, A. Wickenbrock, D. Budker, A. Gali, M. Trupke, F. Jelezko, M. Nesladek, *Semicond. Semimetals* **2021**, *104*, 105.
- [26] X. D. Chen, C. L. Zou, F. W. Sun, G. C. Guo, *Appl. Phys. Lett.* **2013**, *103*, 013112.
- [27] B. J. Shields, Q. P. Unterreithmeier, N. P. de Leon, H. Park, M. D. Lukin, *Phys. Rev. Lett.* **2015**, *114*, 136402.
- [28] D. A. Hopper, R. R. Grote, A. L. Exarhos, L. C. Bassett, *Phys. Rev. B* **2016**, *94*, 241201(R).
- [29] K. Jensen, V. M. Acosta, A. Jarmola, D. Budker, *Phys. Rev. B: Condens. Matter Mater. Phys.* **2013**, *87*, 014115.
- [30] D. Hopper, H. Shulevitz, L. Bassett, *Micromachines* **2018**, *9*, 437.
- [31] L. Razinkovas, M. Maciaszek, F. Reinhard, M. W. Doherty, A. Alkaskas, *Phys. Rev. B* **2021**, *104*, 235301.
- [32] K. Iakoubovskii, G. J. Adriaenssens, M. Nesladek, *J. Phys.: Condens. Matter* **2000**, *12*, 189.
- [33] A. T. Collins, *J. Phys.: Condens. Matter* **2002**, *14*, 3743.
- [34] A. Wotherspoon, J. W. Steeds, B. Catmull, J. Butler, *Diamond Relat. Mater.* **2003**, *12*, 652.
- [35] Y. Doi, T. Fukui, H. Kato, T. Makino, S. Yamasaki, T. Tashima, H. Morishita, S. Miwa, F. Jelezko, Y. Suzuki, N. Mizuochi, *Phys. Rev. B* **2016**, *93*, 081203(R).
- [36] S. Dhomkar, H. Jayakumar, P. R. Zangara, C. A. Meriles, *Nano Lett.* **2018**, *18*, 4046.
- [37] D. Bluvstein, Z. Zhang, A. C. B. Jayich, *Phys. Rev. Lett.* **2019**, *122*, 076101.
- [38] J. Chen, S. Lourette, K. Rezai, T. Hoelzer, M. Lake, M. Nesladek, L.-S. Bouchard, P. Hemmer, D. Budker, *Appl. Phys. Lett.* **2017**, *110*, 011108.
- [39] H. Jayakumar, J. Henshaw, S. Dhomkar, D. Pagliero, A. Laraoui, N. B. Manson, R. Albu, M. W. Doherty, C. A. Meriles, *Nat. Commun.* **2016**, *7*, 12660.
- [40] J.-P. Chou, Z. Bodrog, A. Gali, *Phys. Rev. Lett.* **2018**, *120*, 136401.
- [41] N. B. Manson, M. Hedges, M. S. J. Barson, R. Ahlefeldt, M. W. Doherty, H. Abe, T. Ohshima, M. J. Sellars, *New J. Phys.* **2018**, *20*, 113037.
- [42] R. U. A. Khan, B. L. Cann, P. M. Martineau, J. Samartseva, J. J. P. Freeth, S. J. Sibley, C. B. Hartland, M. E. Newton, H. K. Dhillon, D. J. Twitchen, *J. Phys.: Condens. Matter* **2013**, *25*, 275801.
- [43] A. M. Edmonds, U. F. S. D'Haenens-Johansson, R. J. Cruddace, M. E. Newton, K.-M. C. Fu, C. Santori, R. G. Beausoleil, D. J. Twitchen, M. L. Markham, *Phys. Rev. B* **2012**, *86*, 035201.
- [44] V. M. Acosta, E. Bauch, M. P. Ledbetter, C. Santori, K. M. C. Fu, P. E. Barclay, R. G. Beausoleil, H. Linget, J. F. Roch, F. Treussart, S. Chemerisov, W. Gawlik, D. Budker, *Phys. Rev. B: Condens. Matter Mater. Phys.* **2009**, *80*, 115202.
- [45] R. Jones, J. P. Goss, P. R. Briddon, *Phys. Rev. B: Condens. Matter Mater. Phys.* **2009**, *80*, 033205.
- [46] L. Hacquebard, L. Childress, *Phys. Rev. A* **2018**, *97*, 063408.
- [47] X. D. Chen, S. Li, A. Shen, Y. Dong, C. H. Dong, G. C. Guo, F. W. Sun, *Phys. Rev. Appl.* **2017**, *7*, 014008.
- [48] J. Soucek, et al., *manuscript in preparation*.
- [49] K. Okumura, J. Mort, M. A. Machonkin, *Philos. Mag. Lett.* **1992**, *65*, 105.
- [50] E. Rohrer, C. Graeff, R. Janssen, C. Nebel, M. Stutzmann, H. Güttler, R. Zachai, *Phys. Rev. B: Condens. Matter Mater. Phys.* **1996**, *54*, 7874.
- [51] M. Nesladek, L. M. Stals, A. Stesmans, K. Iakoubovskij, G. J. Adriaenssens, J. Rosa, M. Vaněček, *Appl. Phys. Lett.* **1998**, *72*, 3306.
- [52] O. Lehtinen, B. Naydenov, P. Börner, K. Melentjevic, C. Müller, L. P. McGuinness, S. Pezzagna, J. Meijer, U. Kaiser, F. Jelezko, *Phys. Rev. B* **2016**, *93*, 035202.
- [53] P. Deák, B. Aradi, M. Kaviani, T. Frauenheim, A. Gali, *Phys. Rev. B* **2014**, *89*, 075203.
- [54] C. K. Lin, H. C. Chang, M. Hayashi, S. H. Lin, *Chem. Phys. Lett.* **2009**, *475*, 68.
- [55] M. N. R. Ashfold, J. P. Goss, B. L. Green, P. W. May, M. E. Newton, C. V. Peaker, *Chem. Rev.* **2020**, *120*, 5745.